© 2014. Published by The Company of Biologists Ltd | Journal of Cell Science (2014) 000, 000–000 doi:10.1242/jcs.164814

CORRECTION

Actin-binding proteins differentially regulate endothelial cell stiffness, ICAM-1 function and neutrophil transmigration

Antje Schaefer, Joost te Riet, Katja Ritz, Mark Hoogenboezem, Eloise C. Anthony, Frederik P. J. Mul, Carlie J. de Vries, Mat J. Daemen, Carl G. Figdor, Jaap D. van Buul and Peter L. Hordijk

There was an error published in *J. Cell Sci.* **127**, 4470-4482.

The received date for this article should be 6 April 2014.

We apologise to the authors and readers for any confusion that this error might have caused.

© 2014. Published by The Company of Biologists Ltd | Journal of Cell Science (2014) 127, 4470–4482 doi:10.1242/jcs.154708

RESEARCH ARTICLE

Actin-binding proteins differentially regulate endothelial cell stiffness, ICAM-1 function and neutrophil transmigration

Antje Schaefer[1,*], Joost te Riet[2], Katja Ritz[3], Mark Hoogenboezem[1], Eloise C. Anthony[1], Frederik P. J. Mul[1], Carlie J. de Vries[4], Mat J. Daemen[3], Carl G. Figdor[2], Jaap D. van Buul[1] and Peter L. Hordijk[1,*]

ABSTRACT

Chronic vascular inflammation is driven by interactions between activated leukocytes and the endothelium. Leukocyte β2-integrins bind to endothelial intercellular adhesion molecule 1 (ICAM-1), which allows leukocyte spreading, crawling and transendothelial migration. Leukocytes scan the vascular endothelium for permissive sites to transmigrate, which suggests that there is apical membrane heterogeneity within the endothelium. However, the molecular basis for this heterogeneity is unknown. Leukocyte adhesion induces ICAM-1 clustering, which promotes its association to the actin-binding proteins filamin B, α-actinin-4 and cortactin. We show that these endothelial proteins differentially control adhesion, spreading and transmigration of neutrophils. Loss of filamin B, α-actinin-4 and cortactin revealed adaptor-specific effects on a nuclear-to-peripheral gradient of endothelial cell stiffness. By contrast, increasing endothelial cell stiffness stimulates ICAM-1 function. We identify endothelial α-actinin-4 as a key regulator of endothelial cell stiffness and of ICAM-1-mediated neutrophil transmigration. Finally, we found that the endothelial lining of human and murine atherosclerotic plaques shows elevated levels of α-actinin-4. These results identify endothelial cell stiffness as an important regulator of endothelial surface heterogeneity and of ICAM-1 function, which in turn controls the adhesion and transmigration of neutrophils.

KEY WORDS: Adhesion, Endothelium, Inflammation, Transmigration

INTRODUCTION

Cardiovascular diseases, including atherosclerosis, represent major health problems in the human population and are caused primarily by chronic vascular inflammation. This inflammation is characterized by an increased influx of activated leukocytes, which is stimulated by age-related stiffening of the vascular wall (Huynh et al., 2011). Chronic, as well as acute, inflammation is driven by interactions between activated leukocytes and the endothelium, which lines the veins and arteries. The migration of activated leukocytes, such as neutrophils, across the inflamed endothelium involves adhesion and spreading followed by the breaching of endothelial, pericyte and basement membrane barriers (Nourshargh et al., 2010). Firm adhesion and spreading of neutrophils is mediated by binding of β2-integrins to their endothelial ligand ICAM-1. The adhesive function of ICAM-1 requires its clustering, a consequence of ICAM-1 binding to the β2-integrins Mac1 (macrophage 1 antigen; also known as αMβ2 integrin) or LFA1 (leukocyte function-associated antigen 1; also known as αLβ2 integrin).

In the endothelium of the blood vessel wall, ICAM-1 clustering induces its association with cytoplasmic actin-binding adaptor proteins that link ICAM-1 to the F-actin cytoskeleton. These adhesion complexes promote formation of local membrane protrusions that surround adherent leukocytes and allow efficient leukocyte transendothelial migration (TEM) (Barreiro et al., 2002; van Buul et al., 2007a). Actin-binding proteins, such as filamin B, cortactin and α-actinin-4, associate with the intracellular portion of ICAM-1 (Carpén et al., 1992; Kanters et al., 2008; Oh et al., 2007; Yang et al., 2006). Deletion of this region inhibits ICAM-1-dependent leukocyte adhesion and TEM (Lyck et al., 2003). Each of these adaptor proteins regulates actin dynamics in different ways. Filamins crosslink actin fibers in an orthogonal fashion and increase cortical membrane stability (Stossel et al., 2001). Cortactin promotes F-actin filament branching by activating the Arp2/3 complex, which drives membrane protrusion and cell migration (Kirkbride et al., 2011). α-Actinin-4 is an anti-parallel homodimer that crosslinks F-actin filaments (Courson and Rock, 2010). Thus, differences in the formation of ICAM-1-based complexes might allow different local environments to be presented to adherent neutrophils.

Firmly adherent leukocytes spread and crawl over the vascular endothelium, scanning the apical cell surface for permissive sites for TEM (Nourshargh et al., 2010). This decision-making behaviour suggests that these adherent cells sense apical membrane heterogeneity within the vascular endothelium. However, the molecular basis for this heterogeneity is unknown. We questioned here whether apical endothelial heterogeneity, resulting from distinct complexes of ICAM-1 with different actin-binding proteins, controls neutrophil TEM. Neither the presence of such parallel ICAM-1-regulating complexes, nor their functional relevance for neutrophil TEM, has been investigated previously.

Using a multidisciplinary approach, we show that ICAM-1 forms molecularly and functionally distinct complexes with filamin B, α-actinin-4 and cortactin in inflamed primary human endothelial cells. We found that these adaptor proteins, and in particular α-actinin-4, differentially control endothelial cell stiffness, which is presented as a nuclear-(low)-to-peripheral (high) gradient to ICAM-1-bound neutrophils. Finally, we show

[1]Department of Molecular Cell Biology, Sanquin Research and Landsteiner Laboratory, Academic Medical Center and Swammerdam Institute of Life Sciences, University of Amsterdam, 1066 CX Amsterdam, The Netherlands. [2]Department of Tumor Immunology, Nijmegen Centre for Molecular Life Sciences, Radboud University Nijmegen Medical Centre, Nijmegen 6525 GA, The Netherlands. [3]Department of Pathology, Academic Medical Center, University of Amsterdam, 1105 AZ Amsterdam, The Netherlands. [4]Department of Medical Biochemistry, Academic Medical Center, University of Amsterdam, 1105 AZ Amsterdam, The Netherlands.

*Authors for correspondence (a.schaefer@sanquin.nl; p.hordijk@sanquin.nl)

Received 6 April 2013; Accepted 22 July 2014

Journal of Cell Science

Journal of Cell Science (2014) 127, 4470–4482 doi:10.1242/jcs.154708

that the endothelium, lining atherosclerotic plaques in mice and humans, expresses elevated levels of α-actinin-4 protein. Taken together, our findings identify α-actinin-4 as an important regulator of endothelial cell stiffness and of ICAM-1-mediated neutrophil TEM.

RESULTS

Loss of endothelial actin-binding proteins differentially reduces neutrophil TEM

To define the specific function of ICAM-1-based adhesion complexes in neutrophil spreading, crawling and TEM (Fig. 1A), we reduced the expression of filamin B, α-actinin-4 and cortactin in primary human endothelial cells using validated small interfering RNAs (siRNAs) (supplementary material Fig. S1A) (Craig et al., 2007; Kanters et al., 2008; Yang et al., 2006). Next, the endothelial cells were stimulated with the inflammatory cytokine tumour necrosis factor α (TNFα), and we quantified polarization, spreading, adhesion and TEM of primary human neutrophils, which adhere through their β2-integrins, under physiological flow. Reduction of either of the three adaptor proteins significantly reduced neutrophil spreading (Fig. 1B; supplementary material Movies 1, 2) and polarization (Fig. 1C), with a consequent reduction of adhesion and TEM (Fig. 1D; supplementary material Fig. S1B,C). Depletion of endothelial α-actinin-4 induced the most pronounced effects in all these experiments. Moreover, the extent of inhibition of TEM correlated directly with the level of siRNA-mediated reduction of α-actinin-4 expression throughout the individual experiments (supplementary material Fig. S1D). siRNA-mediated loss of the α-actinin-4 homologue α-actinin-1 did not affect neutrophil spreading or TEM (supplementary material Fig. S1E). Thus, endothelial actin-binding proteins differentially control ICAM-1-dependent neutrophil adhesion, spreading, polarization and TEM.

Adaptor-specific dynamics within the ICAM-1 complex

Next, we used magnetic beads coated with an anti-ICAM-1-antibody to isolate ICAM-1–adaptor protein complexes (Kanters et al., 2008). Adhesion of these beads to intact cells prior to extraction mimics leukocyte adhesion and will cluster cell surface ICAM-1. In contrast, addition of these beads to lysed cells allows isolation of non-clustered ICAM-1. We found that filamin B, α-actinin-4 and cortactin specifically bound to clustered, but not to

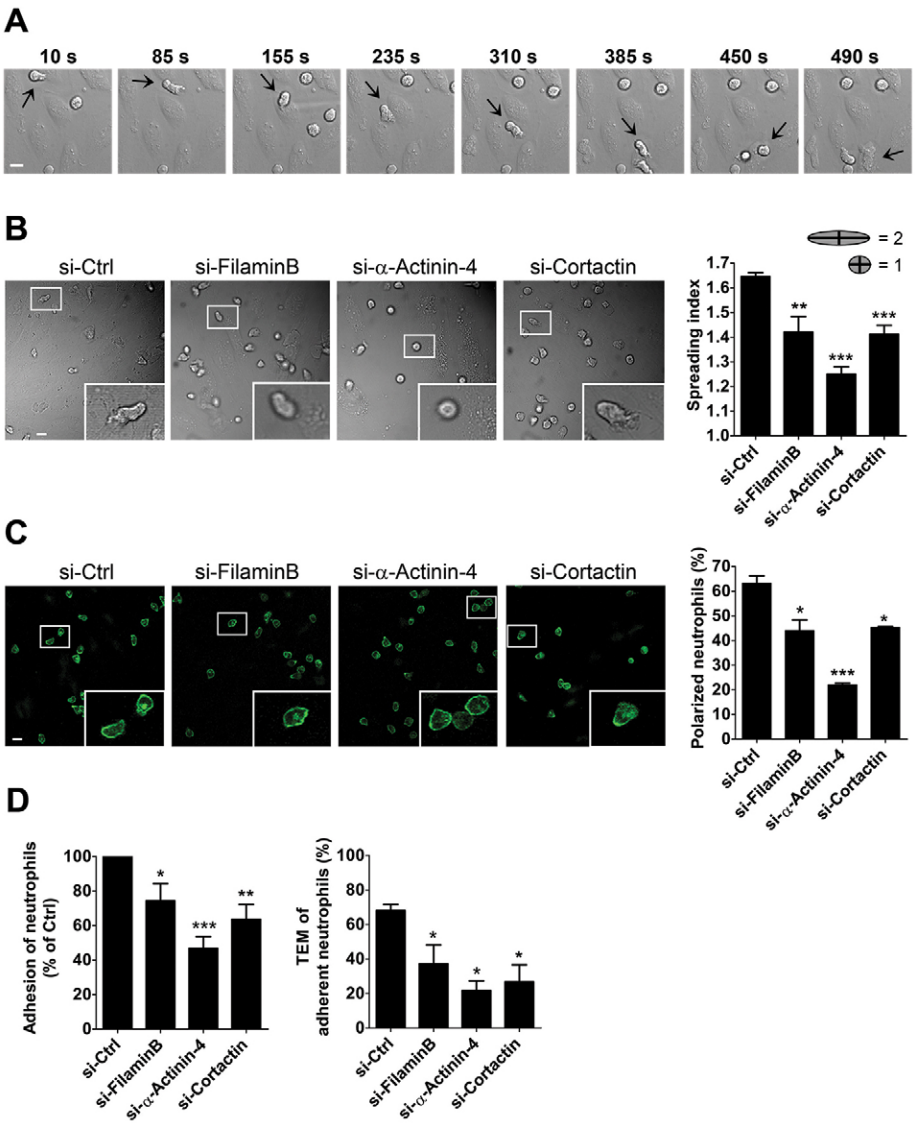

Fig. 1. Endothelial ICAM-1–binding proteins regulate polarization, spreading, adhesion and TEM of neutrophils. (A) A human neutrophil scans the surface of a TNFα-treated HUVEC monolayer, prior to TEM. TEM occurs at between 450 and 490 s. Images are stills from a representative DIC-based live-cell imaging study under physiological flow. (B) A TNFα-treated HUVEC monolayer was transfected with the indicated siRNA (si-) and spreading of human neutrophils was observed by DIC. Images are stills from a representative live-cell imaging experiment (supplementary material Movies 1, 2). Insets show magnifications of typical neutrophil phenotypes. Quantification of spreading index at t=6 min following neutrophil addition (right panel) shows that loss of α-actinin-4 caused the most pronounced defect (n=5 independent experiments, 8–17 neutrophils per group). (C) At the end of the experiments in B, after 25 min, cells were fixed and neutrophils were immunostained for ICAM-3 as a polarity marker. Insets show magnifications of typical ICAM-3 distributions. Quantification (right panel) shows that loss of endothelial α-actinin-4 caused the most significant reduction in polarization (n=3, 14–71 neutrophils per group). (D) Depletion of α-actinin-4 also results in the strongest reduction in adhesion (left panel) and TEM (right) of adherent neutrophils across a TNFα-treated HUVEC monolayer under physiological flow, measured at 30 min following neutrophil addition (n=5, 148–255 neutrophils per group). Scale bars: 10 μm. Data are mean±s.e.m., *P<0.05; **P<0.01, ***P<0.001 (Student's t-test).

Journal of Cell Science (2014) 127, 4470–4482 doi:10.1242/jcs.154708

non-clustered ICAM-1 in TNFα-activated primary human endothelial cells (supplementary material Fig. S2A,B). In line with this result and previous studies (Carpén et al., 1992; Celli et al., 2006; Kanters et al., 2008; Yang et al., 2006), we found that filamin B, α-actinin-4 and cortactin associated with a peptide encoding the ICAM-1 intracellular domain (supplementary material Fig. S2C). Taken together, these data show that whereas the intracellular domain of ICAM-1 is sufficient for the association, the clustering of ICAM-1 in live cells is necessary for efficient binding to these adaptor proteins.

We then studied the dynamics of these ICAM-1–adaptor protein complexes in live TNFα-stimulated primary human endothelial cells expressing GFP-tagged fusion proteins. We found that α-actinin-4–GFP is, similar to filamin-B–GFP (Kanters et al., 2008) and cortactin–GFP (Schnoor et al., 2011; Yang et al., 2006), recruited to adherent and transmigrating neutrophils and to anti-ICAM-1 beads (Fig. 2A,B; supplementary material Movies 3, 4). This recruitment was paralleled by the local accumulation of ICAM-1 and F-actin (supplementary material Fig. S2D). Quantification (supplementary material Fig. S2E) revealed sequential recruitment of the adaptor proteins, with α-actinin-4–GFP being recruited with the same kinetics as ICAM-1–GFP, whereas cortactin–GFP and filamin B–GFP were recruited slower with lag times of ∼200 s and ∼400 s, respectively (Fig. 2B). Similar data were obtained in endothelial cells that co-expressed ICAM-1–mCherry with any of the GFP-linked adaptor proteins (data not shown). Moreover, we did not detect changes in cytoskeletal organization upon ectopic expression of the GFP-tagged adaptor proteins (A.S., unpublished results). To study the mobility of the GFP-tagged adaptors following recruitment to

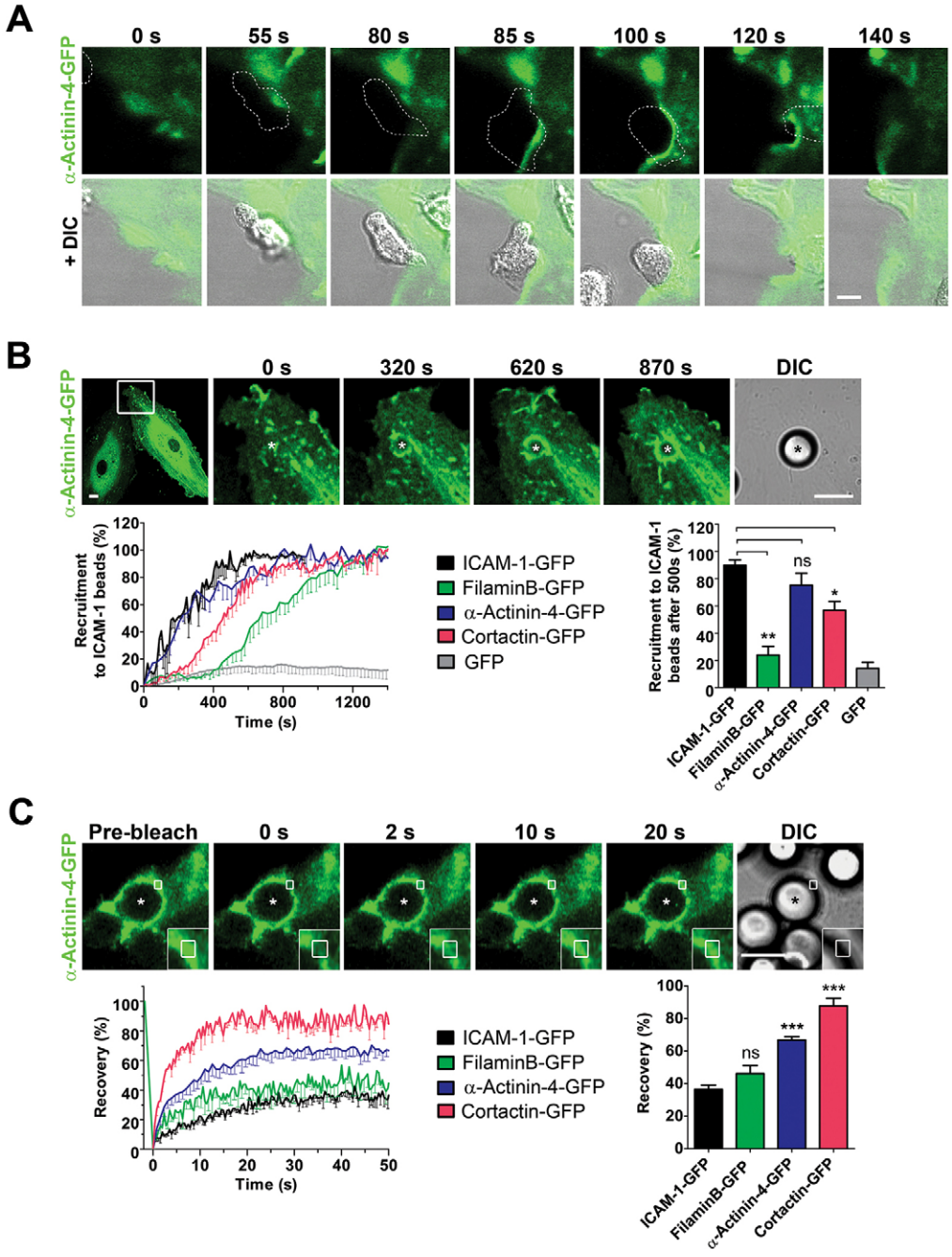

Fig. 2. Dynamics of actin-binding proteins in the ICAM-1 complex. (A) α-actinin-4–GFP in TNFα-treated HUVEC is recruited to an adherent and transmigrating human neutrophil. Images are stills from a representative live-cell imaging experiment (n=4). The neutrophil (dotted line in GFP images) transmigrates after 85 s (supplementary material Movie 3). Note that this experiment was performed using a monolayer of endothelial cells: the cell in the left portion of the images did not express α-actinin-4–GFP. (B) Upon addition of anti-ICAM-1 beads (DIC image) to TNFα-treated HUVECs transfected with ICAM-1–GFP or the indicated GFP-tagged adaptor, recruitment of fusion proteins was recorded for 25 min. Still images are shown for α-actinin-4–GFP (supplementary material Movie 4). Quantification (lower left panel) is shown for recruitment of ICAM-1–GFP (n=3), filamin-B–GFP (n=3), α-actinin-4–GFP (n=4), cortactin–GFP (n=5) and GFP alone (n=3, t=0 s is when beads were added). Recruitment at t=500 s is shown in the bar graph (lower right panel). (C) Mobility of GFP-tagged adaptors and ICAM-1–GFP was analysed by FRAP following the recruitment to anti-ICAM-1 beads. Still images show bleaching (see insets) and recovery of α-actinin-4–GFP. Recovery curves (lower left panel) and bar graph (lower right panel) of the mobile fraction, based on the GFP signal after 40–50 s following bleaching (α-actinin-4–GFP, n=4; cortactin–GFP, n=3; filamin-B--GFP, n=5; ICAM-1–GFP, n=4). Each independent experiment is an average of two or three cells with one or two rings per cell. Data are mean±s.e.m. ns, not significant, *P<0.05; **P<0.01, ***P<0.001 (Student's t-test). The asterisk in B and C indicates the bead position. Scale bars: 5 μm (A); 10 μm (B,C).

Journal of Cell Science (2014) 127, 4470–4482 doi:10.1242/jcs.154708

clustered ICAM-1, we performed fluorescence recovery after photobleaching (FRAP) experiments. We found that filamin B showed the lowest mobility in the clustered ICAM-1 complex (Fig. 2C). This is in marked contrast to cortactin, which showed the highest mobility, with α-actinin-4 displaying an intermediary phenotype. These results show that each of these actin-binding adaptor proteins, which are also heterogeneously distributed in primary endothelial cells (supplementary material Fig. S2F), show specific dynamics both during recruitment to clustered ICAM-1 and following complex formation.

ICAM-1 forms molecularly distinct complexes with adaptor proteins

To test whether filamin B, α-actinin-4 or cortactin bound independently to clustered ICAM-1, we performed siRNA-based reduction of expression of these proteins in TNFα-activated endothelial cells, followed by isolation of clustered ICAM-1. We found that loss of neither of these adaptor proteins impaired ICAM-1 binding to the others, supporting the notion that ICAM-1 clustering induces the formation of molecularly distinct, F-actin-linked adhesion complexes (Fig. 3A).

Next, we investigated which regions within the intracellular domain of ICAM-1 bind to these adaptor proteins. The structure model of the intracellular domain of ICAM-1 shows that the highly conserved membrane-proximal region forms an α-helix and the distal, much less conserved region, is unstructured (Fig. 3B). Previous studies have identified the cluster of basic residues in the α-helical region as being necessary to regulate the ICAM-1–α-actinin-4 interaction (Carpén et al., 1992; Celli et al., 2006). However, published data (Oh et al., 2007) and our own findings (unpublished data) show that mutation of the residues Lys508, Lys510 and Lys511 to alanine residues inhibits ICAM-1 surface expression and clustering, precluding efficient association to any of the adaptor proteins in the cell.

The amino acid sequence of the ICAM-1 intracellular domain differs for almost 40% of residues (11 residues out of 28) between mouse and human, mainly in the unstructured membrane-distal part (Fig. 3B). Whereas binding of cortactin to peptides encoding the human or murine sequence was similar, interaction of α-actinin-4 and filamin B to the mouse ICAM-1 peptide was significantly less as compared to the human peptide (supplementary material Fig. S3A). This suggests that the membrane-distal unstructured portion of the intracellular domain mediates these interactions. As described for other protein–protein interactions (Bishop and Hall, 2000), such a region might become structured upon adaptor protein binding, possibly in an adaptor-specific fashion. This region contains two lysine residues in human ICAM-1 (Fig. 3B). Although Lys524 is highly conserved, Lys519 is a glutamate in the murine sequence. We mutated both lysine residues to alanine residues in full-length human ICAM-1 and analysed adaptor protein binding following ICAM-1 clustering. Whereas binding to α-actinin-4 required both Lys519 and Lys524, binding to filamin B was dependent on Lys519 and, in contrast, binding to cortactin was unaffected (Fig. 3C). Control experiments confirmed that surface expression and clustering of these ICAM-1 mutants and of wild-type (WT) ICAM-1 was similar (supplementary material Fig. S3B).

Given that depletion of α-actinin-4 affected neutrophil TEM most significantly (Fig. 1), we analysed α-actinin-4 binding to ICAM-1 in more detail. Purified human α-actinin-4 bound directly and specifically to a biotinylated peptide encoding the intracellular domain of human ICAM-1-WT, as previously published (Carpén et al., 1992), but less strong to the peptide with the K519A-K524A mutation (supplementary material Fig. S3C), which is in line with the results shown in Fig. 3C. Secondly, we found that expression of the full-length ICAM-1 K519A-K524A mutant in TNFα-activated primary human endothelial cells impaired neutrophil polarization and spreading (Fig. 3D,E). These results show that the intracellular domain of ICAM-1 encodes adaptor-specific binding sites, which allows formation of molecularly distinct complexes with filamin B, α-actinin-4 and cortactin.

The actomyosin network differentially regulates ICAM-1-adaptor binding

ICAM-1 clustering in endothelial cells regulates cytoskeletal dynamics, including Rho-mediated actomyosin-based contractility (Etienne et al., 1998; Lyck et al., 2003; van Buul et al., 2007b). Conversely, Rho signalling is known to control ICAM-1 function and leukocyte adhesion to endothelial cells (Wójciak-Stothard et al., 1999). We analysed the role of Rho signalling further by inhibiting the Rho-effector Rho kinase (ROCK) with Y27632 and myosin II with blebbistatin. Inhibition of ROCK or myosin II significantly reduced the association of filamin B and α-actinin-4, but not that of cortactin, to ICAM-1 (Fig. 4A; supplementary material Fig. S3D). Similarly, destabilizing the F-actin cytoskeleton with low concentrations of cytochalasin B reduced the interaction of filamin B, α-actinin-4 and actin with clustered ICAM-1 whereas binding of cortactin increased 2–3-fold (Fig. 4B; supplementary material Fig. S3E,F). Stabilizing the F-actin network with jasplakinolide promoted the interaction of α-actinin-4, cortactin and actin with ICAM-1, but reduced the binding of filamin B (Fig. 4C; supplementary material Fig. S3G). Importantly, the amount of clustered ICAM-1 that was isolated, as well as monolayer integrity was unaffected under any of these conditions (supplementary material Fig. S3D–G) (van Buul et al., 2010a). Taken together, these experiments show that ICAM-1 bound to the different actin-binding adaptor proteins is differentially regulated by F-actin (de)polymerization and contractility.

Actin-binding proteins differentially regulate endothelial cell stiffness

Filamin B, α-actinin-4 and cortactin control the organization of the F-actin cytoskeleton in different ways, such as by crosslinking (α-actinin-4) or formation of branching (cortactin). These differences in cytoskeletal organization might translate into local effects on endothelial cell stiffness, which might control spreading and migration of adherent neutrophils (Oakes et al., 2009; Raab et al., 2012). We therefore used atomic force microscopy (AFM) to measure changes in endothelial cell stiffness following siRNA-mediated depletion of filamin B, α-actinin-4 and cortactin. Note that we used a 10-μm polystyrene bead glued to the cantilever for these measurements. We found that in primary human endothelial cells, the nuclear area is relatively compliant as compared to the stiffer periphery of the cells (Fig. 4D–G). Loss of filamin B had little effect on endothelial cell stiffness, whereas α-actinin-4 significantly decreased endothelial cell peripheral stiffness, reducing the slope of the stiffness gradient provided by the endothelial cell (Fig. 4E,F). Loss of cortactin also reduced peripheral stiffness, but to a lesser extent as compared to α-actinin-4 (Fig. 4G). Finally, we found that depletion of cortactin and especially of α-actinin-4 led to a reduced mechanosensitive response of the

Journal of Cell Science (2014) 127, 4470–4482 doi:10.1242/jcs.154708

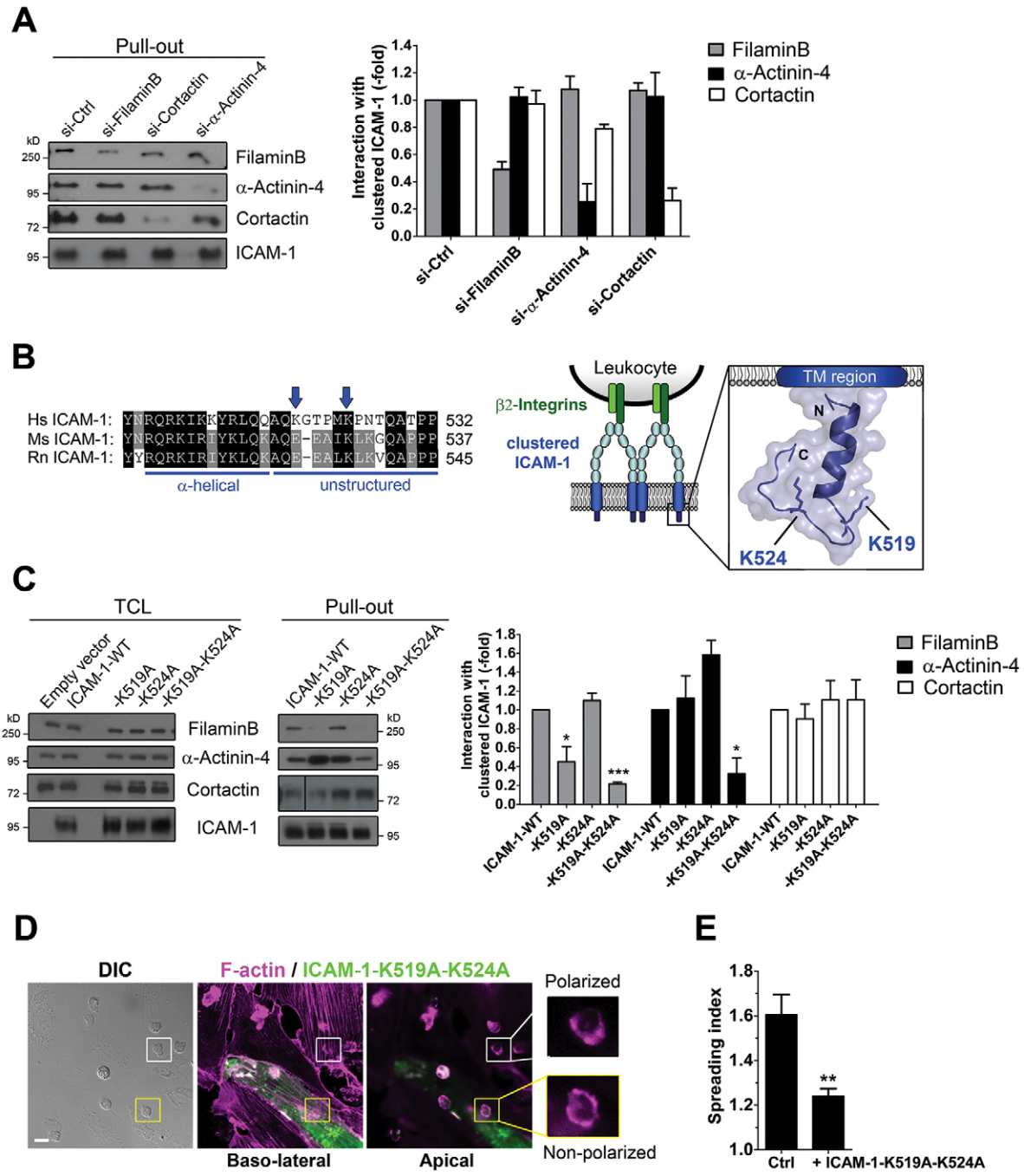

Fig. 3. ICAM-1 forms distinct complexes with filamin B, α-actinin-4 and cortactin. (A) Western blots show that depletion (by siRNA, si-) of filamin B, cortactin or α-actinin-4 in TNFα-treated HUVEC did not affect binding of the other adaptors to ICAM-1 (total cell lysate in supplementary material Fig. S1A). Bar graphs show quantification of the interactions ($n=3$). (B) Sequence alignment of the intracellular ICAM-1 domain from human, mouse and rat (left panel) and the structure model of the human intracellular ICAM-1 domain (right panel). Mutated residues Lys519 and Lys524 are indicated by arrows and in stick representation. TM, transmembrane. (C) Full-length human wild-type (WT) ICAM-1 and indicated mutants were expressed in ICAM-1-deficient HeLa cells, prior to analysis of binding of endogenous filamin B, cortactin and α-actinin-4 to clustered ICAM-1. Western blots show expression in the total cell lysate (TCL, left panel) and binding to ICAM-1 [pull-out, right panel; quantification, bar graph ($n=3$)]. (D,E) Neutrophils were added to TNFα-treated HUVECs transfected with ICAM-1-K519A-K524A. Cells were fixed after 25 min and stained for HA-tagged ICAM-1-K519A-K524A and F-actin (phalloidin). Neutrophils migrating across HUVECs expressing the ICAM-1 K519A-K524A mutant (green) show (D) less polarization, as deduced from the F-actin distribution (images represent one out of two experiments) and (E) less spreading (as calculated in Fig. 1B; $n=2$, 10 neutrophils per group). Scale bar: 10 μm. Data are mean±s.e.m. $^{*}P<0.05$; $^{**}P<0.01$, $^{***}P<0.001$ (Student's *t*-test).

endothelial cells to the AFM probe (Fig. 4H) underscoring the relevance of these adaptor proteins in endothelial cell mechanosignaling.

We observed a pre-existing central-to-peripheral gradient of endothelial cell stiffness (Fig. 4D–G), a phenomenon which has been observed previously using non-TNFα-treated bovine

Journal of Cell Science

Journal of Cell Science (2014) 127, 4470–4482 doi:10.1242/jcs.154708

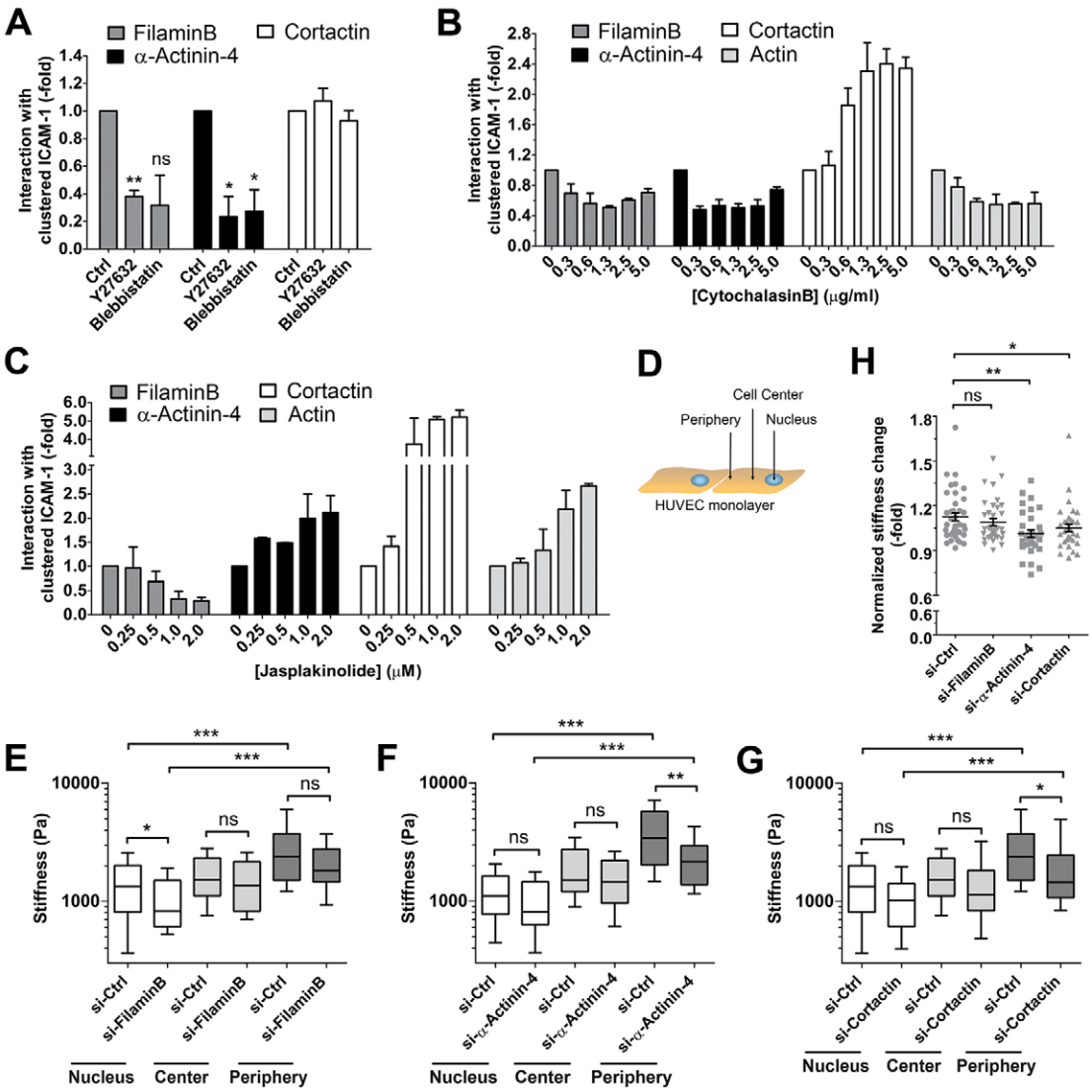

Fig. 4. Adaptor-specific control of endothelial cell stiffness. (A) Inhibition of ROCK by Y27632 or myosin II activity by blebbistatin blocked binding of filamin B and α-actinin-4, but not cortactin, to ICAM-1 (n=2). (B) Destabilization of the F-actin cytoskeleton by cytochalasin B reduced binding of filamin B, α-actinin-4 and actin, but not cortactin, to ICAM-1 (n=3). (C) Stabilization of the F-actin network by jasplakinolide increased binding of cortactin, α-actinin-4 and actin, but not filamin B, to ICAM-1 (n=3). Clustered ICAM-1 levels, western blots for total cell lysate and pull-out are in supplementary material Fig. S3D–G; DMSO was included as control. All experiments were performed with TNFα-stimulated HUVEC monolayers. Data are mean±s.e.m. (D–H) AFM was used to quantify stiffness at the cell periphery, cell centre and above the nucleus of TNFα-treated HUVECs transfected with the indicated siRNA (si-) (n=3, 7–14 cells per condition). (D) Each data point at the indicated position is an average of three single probings at the position shown in the diagram. Quantification of the AFM data for endothelial depletion of (E) filamin B, (F) α-actinin-4 and (G) cortactin is shown in a Box-Whisker diagram. The middle line indicates the median, the box represents the interquartile range and the whiskers represents the 10th and 90th percentiles. (H) Ratio of the first and the last measurement (probing) was calculated for the peripheral endothelial cell stiffness (medial line and error bars represent mean±s.e.m.). ns, not significant; *P<0.05; **P<0.01, ***P<0.001 [Student's t-test (A), Mann–Whitney test (E–H)].

endothelial cells (Sato et al., 2000). Birukova et al. analysed non-TNFα-treated human pulmonary arterial endothelial cells using a 30-nm tip as compared to a 10-μm bead, which is similar to the size of a neutrophil, as used in our assays (Birukova et al., 2009). They detected, in contrast, hardly any differences in elastic module between the periphery and the centre of the resting cells.

ICAM-1 binding and localization of α-actinin-4 correlates with matrix and tissue rigidity

Based on the above findings, we decided to investigate the role of α-actinin-4 in ICAM-1 function in more detail. Live-cell imaging showed that the accumulation of α-actinin-4–GFP and F-actin (LifeAct–GFP) in primary human endothelial cells, in the absence of adherent neutrophils, reflected the stiffness gradient as detected under similar conditions by AFM (supplementary material Fig. S4A). Conversely, we found that loss of α-actinin-4 induced a prominent reorganization of F-actin in primary endothelial cells, marked by a reduction of F-actin cables, as shown by immunofluorescence and by scanning electron microscopy (supplementary material Fig. S4B,C), which is in line with the observed reduction in endothelial cell stiffness upon loss of α-actinin-4 expression (Fig. 4F).

Because we found that the ICAM-1–α-actinin-4 interaction requires Rho-mediated contractility (Fig. 4A), which regulates as well as transduces differences in matrix rigidity (Stroka and Aranda-Espinoza, 2011; Wozniak et al., 2003), we tested whether

Journal of Cell Science (2014) 127, 4470–4482 doi:10.1242/jcs.154708

seeding primary human endothelial cells on matrices with different rigidity would alter the formation of the complex between ICAM-1 and α-actinin-4. We used endothelial cells cultured on relatively stiff (25 kPa) versus soft (0.5 kPa) matrices. These values are in the range reported for stiff (e.g. atherosclerotic vessels) or soft (e.g. brain) tissues, and are also within the range that is relevant for neutrophil TEM *in vitro* and *in vivo* (Huynh et al., 2011; Stroka and Aranda-Espinoza, 2011). We found that culturing TNFα-activated primary human endothelial cells for 48 h on a stiff matrix increased binding of α-actinin-4 to clustered ICAM-1 (Fig. 5A; supplementary material Fig. S4D). In cells on the 25-kPa matrix, α-actinin-4 showed increased co-localization with F-actin stress fibres (Fig. 5B). In agreement with these findings, we found that recruitment of ICAM-1–GFP to anti-ICAM-1 beads, which is dependent on F-actin (van Buul et al., 2010a), was impaired in endothelial cells depleted for α-actinin-4 (supplementary material Fig. S4E). In addition, the effects on ICAM-1 function and neutrophil TEM caused by the loss of α-actinin-4 were not due to altered TNFα-induced signalling, as deduced from the increase in ICAM-1 surface expression or the release of the chemokines IL-6 and IL-8 (supplementary material Fig. S4F,G). We next investigated the expression level and distribution of α-actinin-4 in the endothelial lining of blood vessels of different stiffness. We isolated arteries (aorta) and veins (left superior vena cava) from healthy adult mice and performed an *ex vivo* confocal staining for α-actinin-4, together with PECAM-1 as an endothelial marker. As compared to venous endothelium, α-actinin-4 showed a markedly increased expression in arterial endothelial cells, correlating well with increased stiffness in arteries (Fig. 5C). These findings are indicative for an F-actin-dependent positive feedback loop in which ICAM-1-induced recruitment of α-actinin-4 increases local stiffness that in turn stabilizes the ICAM-1–α-actinin-4 complex.

The above findings suggest that increased vascular stiffness, as documented for ageing or inflamed blood vessels (Huynh et al., 2011), promotes endothelial ICAM-1 function and, as a result, leukocyte adhesion, TEM and inflammation. We therefore investigated α-actinin-4 expression in atherosclerotic lesions, which are characterized by increased stiffness, local inflammation and leukocyte TEM (Huynh et al., 2011; Tracqui et al., 2011). We could readily detect α-actinin-4 in the endothelium, lining the aortas of ApoE$^{-/-}$ mice (Fig. 5D; supplementary material Fig. S4H). To quantify endothelial α-actinin-4, we performed a double-staining with PECAM-1 to mark the endothelium. This analysis showed that α-actinin-4 expression levels were significantly higher in the endothelial lining of atherosclerotic plaques, as compared to the endothelial lining of 'non-plaque' areas in the same murine vessel (Fig. 5E,F). Importantly, we also detected significantly elevated α-actinin-4 levels in the endothelium lining atherosclerotic plaques in human aortas

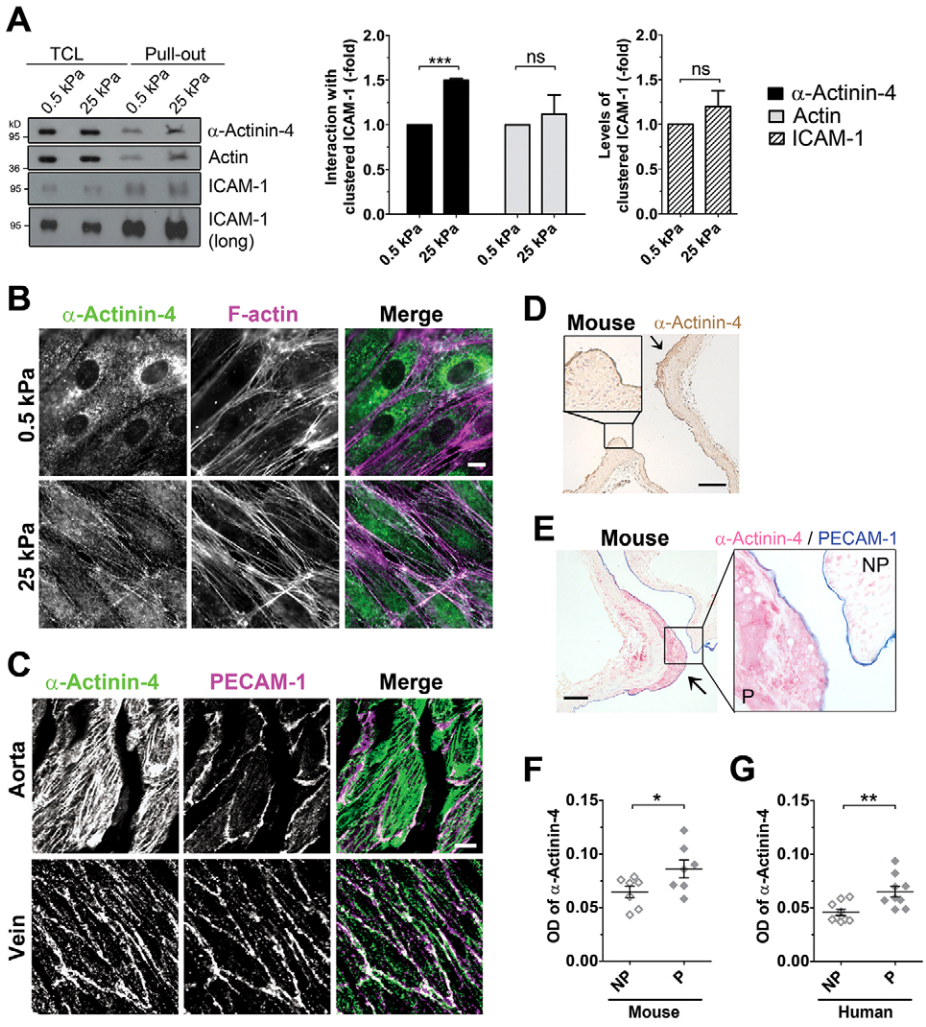

Fig. 5. α-Actinin-4 binding to ICAM-1 and localization correlate with matrix and tissue rigidity. (A) Confluent HUVECs cultured on soft (0.5 kPa) or stiff (25 kPa) matrix were treated with TNFα. Western blots show total cell lysate (TCL) and binding of actin and α-actinin-4 to clustered ICAM-1 (Pull-out). The left bar graph shows quantification of binding; the right bar graph shows clustered ICAM-1 levels (α-actinin-4 $n=2$; actin, ICAM-1 $n=3$). Data are mean±s.e.m. (B) HUVECs were cultured as in A, and fixed and immunostained as indicated. (C) Endothelial lining of an isolated artery (aorta) and vein (left superior vena cava) of wild-type mice, which were fixed and immunostained for α-actinin-4 (green) and PECAM-1 (magenta), as an endothelial marker. (D) The aortic arch of ApoE$^{-/-}$ mice with atherosclerotic lesion (arrow) was analysed by DAB staining. (E–G) Alkaline phosphatase staining was used to quantify α-actinin-4 (red) in the endothelium, marked by PECAM-1 (blue), of murine (E) or human arteries (supplementary material Fig. S4I). α-Actinin-4 levels were quantified in the endothelial region of the atherosclerotic plaque (P, arrow) versus a control, non-plaque (NP) region of similar size in the same vessel of ApoE$^{-/-}$ mice (7 regions, 3 mice) (F) or in human arteries from the same donor (G) (9 regions, 3 patients). Open symbols, non-plaque regions; closed symbols, plaque regions. Line and error bars represent mean±s.e.m. Scale bars: 10 μm. (B,C); 100 μm (D,E). ns, not significant; *$P<0.05$; **$P<0.01$; ***$P<0.001$ [Student's *t*-test (A), Wilcoxon test (F,G)].

Journal of Cell Science (2014) 127, 4470–4482 doi:10.1242/jcs.154708

(Fig. 5G; supplementary material Fig. S4I). Taken together, these data show that *in vitro* matrix stiffness promotes the association of α-actinin-4 to clustered ICAM-1, and that *in vivo* expression of α-actinin-4 is elevated in atherosclerotic plaques, correlating with increased endothelial cell stiffness and leukocyte infiltration in these areas (Tracqui et al., 2011).

DISCUSSION

Here, we performed a comprehensive study on the dynamics, regulation and functional relevance of molecularly and functionally distinct ICAM-1-based adhesion complexes comprising the actin-binding proteins filamin B, α-actinin-4 and cortactin. We show that these actin-binding proteins differentially regulate endothelial cell stiffness as measured by AFM, and control both ICAM-1 clustering and neutrophil TEM. We found that, in contrast to filamin B and cortactin, α-actinin-4 depletion results in the most significant effects in neutrophil adhesion, spreading and TEM. Moreover, α-actinin-4 shows similar kinetics as ICAM-1 upon ICAM-1 clustering and its binding to ICAM-1 is regulated in a similar fashion as the binding of actin to ICAM-1. Finally, α-actinin-4 is important for endothelial cell stiffness and its expression promotes a cell-autonomous stiffness gradient from the nucleus to cell–cell contacts. α-Actinin-4 contains four α-helical spectrin repeats that confer flexibility (Golji et al., 2009). This might allow α-actinin-4 to resist mechanical strain and to induce RhoA signalling and local changes in the F-actin cytoskeleton (Lessey-Morillon et al., 2014). Thus, α-actinin-4 might not only mediate F-actin crosslinking (Courson and Rock, 2010) but might also act as a force-transmitting element, promoting maturation of ICAM-1-based (this study) or integrin-based (Roca-Cusachs et al., 2013) adhesion complexes.

Intriguingly, filamin B hardly influences endothelial cell stiffness, and shows slow dynamics in recruitment to ICAM-1 and within the complex following its association to clustered ICAM-1. Filamin B might sense rather than control endothelial cell stiffness to convert mechanical stimuli into downstream signalling events during leukocyte TEM. Filamin B induces an actin network comparable to an elastic gel (Stossel et al., 2001), and mechanical strain might stretch filamin B, resulting in spatial separation of binding sites for TEM-regulating proteins such as ICAM-1 (Kanters et al., 2008) or the RhoGEF Trio (van Rijssel et al., 2012). A similar regulatory mechanism was recently described for FilGAP (also known as ARHGAP24)- and integrin-binding to filamin A to control cell spreading (Ehrlicher et al., 2011).

Although to a lesser extent than α-actinin-4, cortactin controls peripheral endothelial cell stiffness. Of all three adaptor proteins, cortactin shows the highest mobility in the ICAM-1 complex and its ICAM-1 binding is stimulated by even small changes in F-actin polymerization. Cortactin binds to and activates the Arp2/3 complex to induce F-actin filament branching, which promotes membrane protrusions and cell migration (Kirkbride et al., 2011). Our findings might thus suggest that cortactin is involved in the spatio-temporal control of the Arp2/3 complex during leukocyte TEM.

Previous studies (Oakes et al., 2009; Stroka and Aranda-Espinoza, 2011) have shown that adherent leukocytes, in addition to sensing chemokines, are mechanosensitive to global differences in the stiffness of endothelial cells cultured on rigid or soft matrices. Here, we show that TNFα-treated endothelial cells present a stiffness gradient to adherent leukocytes. Our data indicate that this stiffness gradient is primarily controlled by α-actinin-4, and only slightly by cortactin and not by filamin B. We also show that loss of α-actinin-4 leads to a significant reduction of F-actin cables and ICAM-1 clustering. Based on the recruitment of α-actinin-4 and F-actin by clustered ICAM-1, it is attractive to propose that ICAM-1-mediated leukocyte adhesion further increases α-actinin-4-dependent, local endothelial cell stiffness. Magnetic twisting experiments were recently used to show that pulling on ICAM-1 using antibody-coated beads, increases local stiffness at the level of ICAM-1 (Lessey-Morillon et al., 2014). It is, however, important to underscore that the changes in cellular stiffness that we measured using AFM do not necessarily reflect the stiffness at the level of cell surface ICAM-1. ICAM-1 stiffness is determined by its connection to the cortical actin cytoskeleton, which will be further increased by the integrin-mediated pulling forces exerted by the adherent neutrophil. Optimal stiffness might promote leukocyte spreading on endothelial cells, further increasing the cell–cell contact area and firm adhesion. Leukocyte crawling on the vascular endothelium is essential for efficient TEM *in vitro* and *in vivo* (Phillipson et al., 2006; Schenkel et al., 2004). This crawling is mediated by Mac1 and ICAM-1 and correlates temporally with formation of invadosome-like protrusions (Carman et al., 2007) or ventral filopodia (Shulman et al., 2009). These protrusive structures have been suggested to ‘probe’ the endothelial cell surface in search of permissive sites for transcellular or paracellular diapedesis. It is remains to be proven that such leukocyte probing represents the scanning for areas of optimal stiffness. Intriguingly, most transmigration events occur at the cell periphery, close to or at cell–cell junctions, which is where we measured the highest (optimal) stiffness and α-actinin-4 accumulation. A previous study has shown that presentation of chemokines from intra-endothelial, F-actin-associated vesicle stores is important for TEM of lymphocytes (Shulman et al., 2012). Although TNFα-induced release of IL-6 and IL-8 was unaffected by the α-actinin-4 siRNA, we cannot formerly exclude that the availability of chemokine-containing vesicles is affected under these conditions.

Arterial calcification increases vascular stiffness and correlates with development of atherosclerosis (Huynh et al., 2011). Atherosclerotic plaques are characterized by increased infiltration of monocytes and neutrophils, and by high stiffness (Tracqui et al., 2011). We found that elevated expression of α-actinin-4 correlates positively with regions of atherosclerosis in both mice and humans. α-Actinin-4 promotes cellular stiffness, and its increased expression in endothelial cells on atherosclerotic plaques might increase ICAM-1 function and leukocyte recruitment, supporting a local cycle of rigidity-driven inflammation. Previously, we detected an increase in α-actinin-4 mRNA expression within human atherosclerotic plaques (Sluimer et al., 2007), in line with the data in Fig. 5F,G. Future work might establish α-actinin-4 as a novel marker for (early) atherosclerosis and show whether inhibition of its function reduces local inflammation at the level of the vascular endothelium.

Based on our data, we propose a model (Fig. 6) in which endothelial actin-binding adaptor proteins act in a pro-inflammatory manner by associating to clustered integrin-bound ICAM-1. These proteins not only anchor ICAM-1 to the F-actin cytoskeleton but also differentially control local cytoskeletal dynamics at the sites of leukocyte adhesion. In response to leukocyte-integrin-mediated pulling forces on ICAM-1, these adaptor proteins might further promote local endothelial cell stiffness. This might stabilize ICAM-1-based adhesion, which promotes leukocyte spreading, crawling and diapedesis.

Journal of Cell Science (2014) 127, 4470–4482 doi:10.1242/jcs.154708

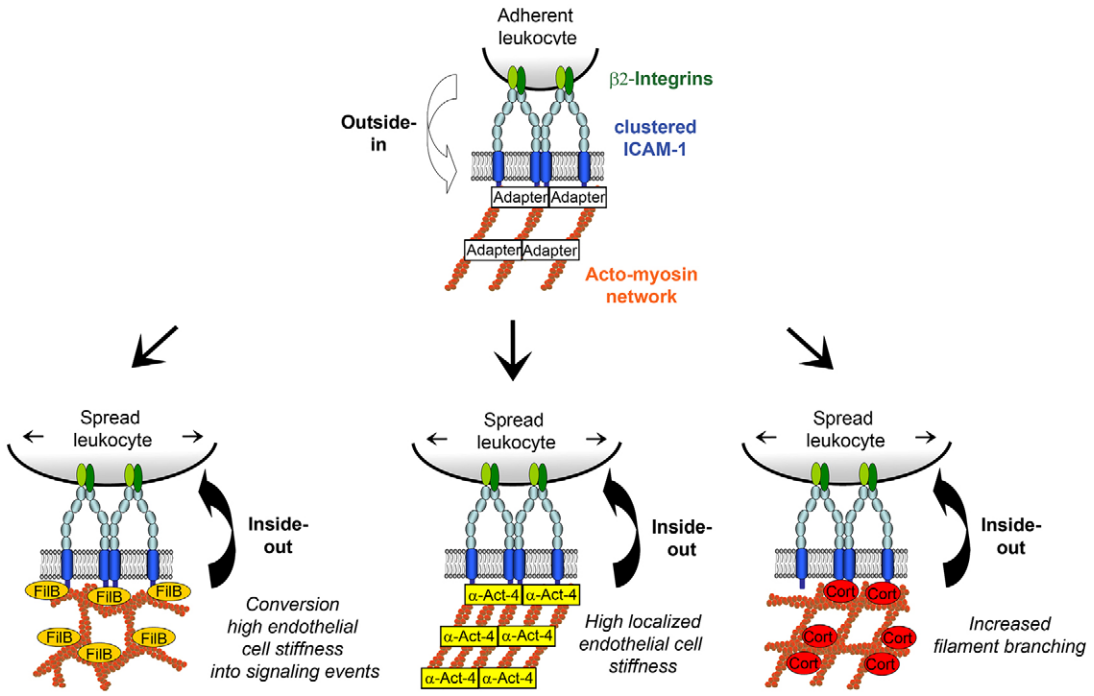

Fig. 6. Adaptor protein-specific control of endothelial cell stiffness is a pro-inflammatory event. Schematic model depicting the positive feedback loop based on the interaction of filamin B, α-actinin-4 or cortactin with integrin-bound clustered ICAM-1. These actin-binding proteins anchor the integrin-bound ICAM-1 complex to the endothelial F-actin cytoskeleton, differentially control cytoskeletal dynamics and might promote endothelial cell stiffness (outside-in signalling). Subsequently, local endothelial cell stiffness might stabilize ICAM-1 adhesion, which promotes efficient leukocyte spreading, crawling and TEM (inside-out signalling).

MATERIALS AND METHODS

Constructs

α-Actinin-4 (a gift from Alain Duperray, University of Grenoble, France) was amplified by PCR using the forward primer 5′-GAGATCGAATTCATGGTGGACTACCACGCGG-3′ and the reverse primer 5′-GAGATCGGTACCGTCAGGTCGCTCTCGCCATAC-3′. The purified PCR product was digested with *Kpn*I/*Eco*RI and directionally cloned into pEGFP-N2 (Clontech), which was digested in the same fashion. Human cortactin (gift from Ed Schuuring, University of Groningen, The Netherlands) was cloned into pEGFP-N2 using the same method and reagents, but with the forward primer 5′-GAGATCGAATTCATGTGGAAAGCTTCAGCAGG-3′ and the reverse primer 5′-ATCGGTACCGTCTGCCGCAGCTCCACATAG-3′. Human filamin-B–GFP was a kind gift from Arnoud Sonnenberg, (Netherlands Cancer Institute, Amsterdam). Human ICAM-1–GFP was a kind gift from Francisco Sanchez-Madrid (University of Madrid, Spain). ICAM-1–mCherry (van Buul et al., 2010b) and LifeAct–GFP (Riedl et al., 2008) were previously described. To generate ICAM-1–HA constructs, a HA tag was cloned into pcDNA3.1zeo (Invitrogen) using a linker which was generated by mixing equal amounts of the primers 5′-GAGATCGCTAGCATGTCTAGATACCCATACGATGTTCCAGATTACGCTAAGCTTTAGATAACTGAGGGCCCGAGATC-3′ and 5′-GATCTCGGGCCCTCAGTTATCTAAAGCTTAGCGTAATCTGGAACATCGTATGGGTATCTAGACATGCTAGCGATCTC-3′. The mix was heated to 100°C and allowed to cool slowly back to room temperature for annealing. The linker was cloned into pcDNA3.1zeo with XbaI/ApaI. ICAM-1 was cloned into the newly generated pcDNA-HA using the same PCR cloning method as above with the forward primer 5′-GAGATCGAATTCATGGCTCCCAGCAGCCCCCG-3′ and the reverse primer 5′-GAGATCTCTAGAGGGAGGCGTGGCTTGTGTGTTCG-3′ and the enzymes *Eco*RI/*Xba*I. Lysine mutants were generated with the same restriction enzymes using the same forward primer but different reverse primers (supplementary material Table S1).

Antibodies

Antibodies were against: actin, α-actinin-1 (BM-75.2), GST, HA and α-tubulin (Sigma), cortactin [BD Transduction and Milipore (4F11)], α-actinin-4 (Enzo Life Science), filamin B (Bethyl Laboratories), ICAM-1 and VCAM-1 (Santa Cruz Biotechnology), VE-cadherin [Beckman Coulter (TEA 1/31)], ICAM-3 [Dako (KS128) and Immunotech (1601)] and PECAM-1 [Dako (JC70A) and Dianova (SZ31)]. Alexa-Fluor-488-labelled mouse PECAM was from R&D Systems. Hoechst 33258, phalloidin–Alexa-Fluor-488, -633 and -Texas-Red and secondary Alexa-Fluor-labelled antibodies were purchased from Invitrogen.

Cell culture, treatments and transfections

HeLa cells were cultured at 37°C and under 5% CO_2 (Kanters et al., 2008) and transfected with ICAM-1–HA constructs using Trans IT-LTI (Mirus) according to the manufacturer's recommendations. Empty vector was used as control. Primary human umbilical vein endothelial cells (HUVECs) were purchased from Lonza and cultured on fibronectin (Sanquin)-coated dishes in EGM-2 medium, supplemented with SingleQuots (Lonza) at 37°C and under 5% CO_2 until passage 8. Unless stated otherwise, HUVECs were stimulated with 10 ng/ml TNFα (Peprotech EC) for 18 h prior to each experiment. TNFα-stimulated HUVEC monolayers were treated with 100 µM blebbistatin (Sigma) for 30 min, with 10 µM Y27632 (Calbiochem) for 12 min or with indicated concentrations of cytochalasin B (0–5 µg/ml; Sigma) or jasplakinolide (0–2 µM; Calbiochem) for 30 min. DMSO was used as control. HUVECs were transfected with validated siRNAs against filamin B (Kanters et al., 2008), α-actinin-1 (Craig et al., 2007), α-actinin-4 (Craig et al., 2007) or cortactin (Yang et al., 2006). As control, siRNA against luciferase (5′-CGUACGCGGAAUACUUCGA-3′) was used. Oligonucleotides were purchased from Eurogentec. HUVECs were transfected with 1.3 nM siRNA, INTERFERin (Polyplus Transfection) and OptiMEM (Invitrogen) according to the manufacturers' recommendations. Cells were used for assays after 72 h. siRNA no. 2 (A-011988-16) and no. 3 (A-011988-17) against α-actinin-4 were obtained from Dharmacon. HUVECs were transfected by electroporation (Neon Transfection System, Life Technologies) or in the case of ICAM-1-K519A-K524A–HA by Trans IT-LTI (Mirus) according to the manufacturers' recommendations. Cells were used for assays after 48 h.

Journal of Cell Science

Western blot analysis

Samples were analysed by SDS-PAGE and western blotting (van Buul et al., 2010a). Proteins were visualized with horseradish peroxidase (HRP)-labelled antibodies (Dako) and enhanced chemiluminescence (ECL; West Dura, Thermo Fisher Scientific). For quantification, integrated intensity was calculated from the mean value and area using Image J.

Peptides and proteins

Peptides were synthesized using Fmoc-solid-phase chemistry (Netherlands Cancer Institute, Amsterdam). N-terminal biotinylated peptides encode the intracellular domain of human ICAM-1 or VCAM-1 (Kanters et al., 2008), murine ICAM-1 (NH_2-RQRKIRIYKLQKA-QEEAIKLKGQAPPP-COOH) or human ICAM-1-K524A-K519A (NH_2-RQRKIKKYRLQQAQAGTPMAPNTQATPP-COOH). GST and GST–α-actinin-4 in pGEX vectors were expressed in *Escherichia coli* BL21 overnight at 18℃ and purified according to the manufacturers' recommendations (Amersham Biosciences). GST or GST–α-actinin-4 was eluted with 20 mM glutathione, 50 mM Tris-HCl pH 7.4, 150 mM NaCl, 5% glycerol, 5 mM β-mercaptoethanol from glutathione–Sepharose-4B beads and dialyzed twice with the same buffer but without glutathione. Proteins were stored at −80℃ upon flash freezing in liquid nitrogen.

Pulldown assays

To analyse the binding to the intracellular domain of human VCAM-1, ICAM-1 and murine ICAM-1, the synthetic biotinylated peptides were used in pulldown assays (Kanters et al., 2008). TNFα-treated HUVEC monolayers were washed with PBS containing 1 mM $CaCl_2$ and 0.5 mM $MgCl_2$ and lysed for 10 min on ice in NP40-buffer (25 mM Tris-HCl pH 7.4, 100 mM NaCl, 10 mM $MgCl_2$, 10% glycerol and 1% NP40), supplemented with a phosphatase inhibitor cocktail (Sigma) and protease inhibitor mixture tablets (Roche). After cell lysis and centrifugation (10,000 ***g***, 10 min, 4℃), supernatant was incubated with streptavidin–agarose beads (Sigma) and 5 µg biotinylated peptide for 3 h at 4℃ under continuous mixing. Beads were washed five times with NP40 buffer, resuspended in SDS sample buffer and proteins were detected by western blotting. To test for direct binding, the biotinylated peptide encoding the intracellular domain of human wild-type ICAM-1 or its K519A-K524A mutant coupled to streptavidin–agarose beads was incubated with purified GST–α-actinin-4 in NP40-buffer for 1 h at 4℃ under continuous mixing. Beads were washed and resuspended in SDS sample buffer and analysed by western blotting. GST was used as control.

Preparation of antibody-coated beads

For immunofluorescence, 10-µm polystyrene beads (Polysciences) were coated with mouse monoclonal antibody (mAb) anti-ICAM-1 (BBIG-l1; R&D) (Kanters et al., 2008). For pull-out experiments, 10-µm magnetic goat anti-mouse-IgG1 antibody-coated Dynabeads (Invitrogen) were coated with mouse mAb anti-ICAM-1 (BBIG-l1), anti-VCAM-1 (Immunotech) or IgG1 control (Sanquin) according to the manufacturers' protocol.

Pull-out clustering experiments

Pull-out clustering experiments were performed using beads coated with anti-ICAM-1, anti-VCAM-1 or IgG1 control (Kanters et al., 2008). To induce clustering, 45 µl antibody-coated beads were added to HeLa cells or to TNFα-stimulated HUVECs in a 10-cm dish and incubated for 25 min at 37℃ and under 5% CO_2. Cells were washed with PBS containing 1 mM $CaCl_2$ and 0.5 mM $MgCl_2$, lysed for 5 min with RIPA buffer (50 mM Tris-HCl pH 7.4, 150 mM NaCl, 10 mM $MgCl_2$, 1% Triton X-100, 0.1% SDS and 0.25% deoxycholic acid) and incubated for 1 h at 4℃ under continuous mixing. Beads were isolated using a magnetic holder, washed twice with RIPA buffer, three times with NP40 buffer and resuspended in SDS sample buffer. For 'non-clustered' conditions, beads were added to the cells upon cell lysis, washed as described above and resuspended in SDS sample buffer. Protein levels were analysed by western blotting. Quantified signals were normalized to the clustered condition.

Confocal laser scanning microscopy

HUVECs were cultured on fibronectin-coated glass coverslips, washed, fixed, immunostained and mounted as described previously (Kanters et al., 2008). Images were recorded with a Zeiss LSM510-META confocal laser scanning microscope (63×/NA 1.4 oil objective). Image acquisition was performed with the Zen2009 software.

Live-cell confocal imaging

Recruitment to neutrophils

HUVEC monolayers transfected with α-actinin-4–GFP were cultured on fibronectin-coated 30-mm glass coverslips and placed in a heating chamber at 37℃ and under 5% CO_2. GFP and differential interference contrast (DIC) signals were monitored using a Zeiss LSM-510-META confocal laser scanning microscope (63×/NA 1.4 oil objective). After 2 min, 500,000 freshly isolated neutrophils were added and imaging was performed for 40 min with intervals of 5 s and *z*-sections at three positions (2.9-µm intervals).

Recruitment to anti-ICAM-1-coated beads

To study recruitment to anti-ICAM-1-coated beads, HUVECs were transfected as indicated and experiments were performed as described above. Here, beads were added after 2 min and imaging was performed for 25 min with intervals of 10 s. Fluorescence intensity was quantified in a donut-shaped area positioned at the centre of the bead and corrected for background, bleaching and transfection efficiency for each cell, time point and confocal plane using Zen2009 software, Image J and Prism5 (Graphpad). For normalization, the average of the saturated signal was set at 100% and the time point of adding the beads was designated as 0 s.

Protein distribution and cell volume

To determine the distribution of α-actinin-4–GFP and LifeAct–GFP in the context of the cell volume, TNFα-activated HUVECs were transfected with indicated GFP construct and with mCherry vector (volume marker) and cultured until confluency on fibronectin-coated glass slides. Live-cell imaging was performed with a maximal pinhole and a 40× oil objective, using a confocal microscope. Double-transfected cells were analysed using Image J. Fluorescence intensities were corrected for background and the ratio of GFP signal to mCherry signal was determined and shown in a rainbow representation from 0 (black) to 5 (white). For quantification, the ratio of the GFP to the mCherry signal in three regions of the same size was measured and averaged. This was performed for areas at the nucleus, cell centre or periphery of each cell ($n=2$, 10–13 cells per condition).

Fluorescence recovery after photobleaching studies

Upon recruitment to anti-ICAM-1-coated beads, FRAP assays were performed in the area of accumulated fusion protein directly next to the bead. Experiments were performed using 50 iterations with 488-nm laser illumination, at maximum power (25 mW) and a confocal laser scanning microscope. Fluorescence recovery was measured by timelapse imaging for 70 s with intervals of 0.395 s. The signal was corrected for background and bleaching for each cell and time point. For normalization, the average of the saturated signal was set at 100%.

Cell culture on different matrices and widefield microscopy

At 24 h prior to stimulation with TNFα, HUVECs were seeded on collagen-I-coated hydrogels bound to a 10-cm dish (Matrigen), for pull-out experiments, or bound to 10-mm glass bottom in a 35 mm dish (Matrigen), for immunofluorescence. Pull-out assays were performed or cells were fixed and immunostained as described above and analysed using an upright Zeiss ImagerZ2 widefield microscope and the ZenBlue software (Zeiss).

FACS analysis

Cells were detached with Accutase (Sigma), stained with mouse anti-ICAM-1-FITC (R&D) or isotype IgG1 control antibodies (Sanquin) and analysed by flow cytometry (FACS CantoII, BD Biosciences) and Flowjo software (Treestar).

Chemokine-release ELISA studies

Supernatants of HUVEC monolayers (12-well-plate) were analysed using PeliKine human IL-6 and IL-8 ELISA kits (Sanquin) according to the manufacturers' recommendations.

Neutrophil isolation

Polymorphonuclear neutrophils were isolated from whole blood derived from healthy donors (with informed consent) by 1:1 dilution with 10% trisodiumcitrate in PBS (Sigma) and a Ficoll-Paque plus density gradient (GE Healthcare). After erythrocyte lysis in cold lysis buffer (155 mM NH_4Cl, 10 mM $KHCO_3$, 0.1 mM EDTA, pH 7.4), neutrophils were washed once with lysis buffer, once with 10% trisodiumcitrate in PBS and suspended in HEPES medium [20 mM HEPES pH 7.4, 132 mM NaCl, 6 mM KCl, 1 mM $MgSO_4$, 1.2 mM K_2HPO_4, 1 mM $CaCl_2$, 5 mM Glucose (Sigma) and 0.4% human serum albumin (Sanquin)] and kept at room temperature for not longer than 5–6 h until use. Neutrophils were activated by incubation at 37℃ for 15 min.

Neutrophil polarization, spreading, adhesion and TEM studies

HUVECs cultured in a fibronectin-coated 10-cm dish were transfected with the indicated siRNAs. Cells were trypsinized after 32 h and half of them were seeded on a fibronectin-coated 30-mm glass coverslip (Thermo Fisher Scientific) and the other half in a fibronectin-coated µ-slide $VI^{0.4}$ (Ibidi). Cells were cultured for 2 days until confluency and stimulated with TNFα 18 h prior to experiments.

Studies under static conditions

500,000 freshly isolated neutrophils were added to HUVEC monolayers cultured on the coverslip and placed in a heating chamber at 37℃ and under 5% CO_2. Live-cell imaging under static conditions was performed for 25 min with intervals of 10 s using DIC at the confocal microscope (63×/NA 1.4 oil objective). Neutrophil spreading was determined after 6 min by calculating the length–width ratio of the cell. TEM was determined after 25 min in nine random fields by calculating transmigrated cells/(transmigrated+non-transmigrated cells)×100 and was normalized to control. To quantify neutrophil polarization, cells were fixed after 25 min, stained for ICAM-3 and analysed by confocal microscopy (see above). Polarization was calculated as ICAM-3 polarized neutrophils/(polarized+non-polarized cells)×100 in six random fields.

HUVECs transfected with ICAM-1-K519A-524A–HA were cultured on fibronectin-coated 30-mm glass coverslips. 500,000 freshly isolated neutrophils were added under static conditions and cells were fixed after 25 min and analysed by confocal microscopy (see above). Neutrophil spreading was determined by measuring the length–width ratio as described above, using DIC images of four random fields. Cells were stained for F-actin and, for transfected HUVECs, with anti-HA mAb and secondary Alexa-Fluor-labelled antibody. Polarization of adherent neutrophils was determined based on F-actin distribution.

Studies under flow conditions

1×10^6 freshly isolated neutrophils in HEPES medium were perfused over HUVEC monolayers in an Ibidi µ-slide (see above) at 1.0 dyne/cm^2 at 37℃ and under 5% CO_2. After 3 min, solution was replaced by HEPES medium. Live-cell imaging under flow was performed for 30 min at intervals of 10 s and recorded in two random fields using a Zeiss Axiovert 200 widefield microscope (10× objective) and the Zeiss Axiovert 4.7 software. To determine neutrophil adhesion, neutrophils were counted after 6 min upon neutrophil addition to the flow chamber, independent on their transmigration behaviour. Numbers were normalized to those of cells expressing the Ctrl siRNA (set at 100%). Neutrophil TEM was calculated by transmigrated neutrophils/(transmigrated+non-transmigrated cells)×100. Transmigrated neutrophils were distinguished from adherent cells by their bright to phase-dark transition.

Scanning electron microscopy

Confluent TNFα-treated HUVECs transfected as indicated were grown on fibronectin-coated glass coverslips, fixated in McDowell's fixative for 1 h at room temperature, and further processed for scanning electron microscopy (van Buul et al., 2010a). Samples were mounted on aluminium stubs (Quorum Technologies), sputter coated with gold and palladium using the coating unit Emitech K550X (Quorum Technologies) and examined on a PhenomPro scanning electron microscopy (Phenom World).

Atomic force microscopy

TNFα-treated HUVEC monolayers transfected as indicated were cultured in a fibronectin-coated 55-mm glass-bottomed dish (Willco Wells). Cells were probed by AFM in EGM-2 medium at 37℃ on a Catalyst BioScope (Bruker) coupled to a confocal microscope (TCS SP5II; Leica) using the Nanoscope software (Bruker). A 10-µm polystyrene bead (Polysciences, Inc.) was glued to a cantilever (NP-S type D, nominal spring constant of 0.06 N/m; Bruker) by a two-component polyurethane glue (Bison) and dried overnight (Krause et al., 2013). Prior to every stiffness measurement, each newly mounted cantilever was calibrated by measuring the deflection sensitivity on glass and subsequently the thermal tune module was used to determine the spring constant using the thermal noise method (te Riet et al., 2011). All steps were carried out in the same dish. To determine the stiffness, cells were probed three times for every position (cell periphery, centre and above the nucleus) using the DIC signal of the confocal microscope and by applying contact forces of 2 nN for 0.5 s. 7–14 cells in a monolayer were analysed for every condition. Approach-retraction distances and velocities were 5 µm and 5 µm/s in a closed *z*-loop. Force–distance curves were obtained and converted into force-indentation (F-δ) curves (the distance was corrected for the cantilever deflection caused by the piezo movement) to quantify deformation depending on the applied force. F-δ curves were fitted over the 0–1.5 nN range using a custom algorithm written in IgorPro6 (Wavemetrics) to calculate the stiffness with the Hertz model for spheres in contact with a flat surface (Lin et al., 2007):

$$F = \frac{4E\sqrt{R_c}}{3(1-\nu^2)} \times \delta^{\frac{3}{2}},$$

where F, force in Newtons (N); R_c, bead radius in meters (m); E, elastic modulus or stiffness in Pascals (Pa); ν, Poisson ratio of 0.5; and δ, indentation in meters (m). To study the mechanosensitivity at the cell periphery of HUVECs transfected with the indicated siRNAs, the ratio of the F-δ curves of the first and the third probing was calculated and normalized.

Mice

For *ex vivo* staining, arteries (aorta) and veins (left superior vena cava) were isolated from healthy adult mice (FVB background). Mice were purchased from Jackson Laboratories (Bar Harbor, USA). For immunohistochemical stainings, atherosclerotic aortic arches were obtained from five-month-old male $ApoE^{-/-}$ mice (C57BL/6 background, chow diet). Mice were bred by the animal facility at the Academic Medical Center, University of Amsterdam and killed with CO_2 prior to the experiments. Mice were a kind gift of Esther Lutgens (University of Amsterdam, The Nertherlands). Experiments were approved by the Committee for Animal Welfare of the Academic Medical Center, University of Amsterdam and were carried out in compliance with guidelines issued by the Dutch government.

Human tissues

Human aortic material was obtained with informed consent from organ donors, according to protocols approved by the Medical Ethics Committee of the Academic Medical Center, University of Amsterdam.

Immunohistochemical analysis

Mouse and human material was fixed in paraformaldehyde, paraffin-embedded and cut in 5-µm thick sections. Sections were dewaxed in xylene and rehydrated in graded alcohol. Immunohistochemical double stainings were performed as previously described (de Boer et al., 2010). Antibodies for murine and human α-actinin-4 (incubated for 1 h at room temperature), for murine PECAM-1 (clone SZ31, 16 h at 4℃) and for human PECAM-1 (clone JC70A, 16 h at 4℃) were used. Heat-induced epitope antigen retrieval was performed in citrate pH 6.0 (α-actinin-4) or Tris-EDTA pH 9.0 (PECAM-1). As second step, sections were incubated

Journal of Cell Science

with alkaline-phosphatase-conjugated anti-mouse-IgG or rabbit-IgG polymer (Immunologic, 30 min at room temperature) for α-actinin-4 and PECAM-1 (clone JC70A). For PECAM-1 (clone SZ31), sections were incubated with rabbit anti-rat-IgG antibody (Southern Biotech, 30 min at room temperature) followed by alkaline-phosphatase-conjugated anti-rabbit-IgG polymer. α-Actinin-4 reactivity was visualized using VectorRed and PECAM-1 using VectorBlue (Vector Labs). Negative controls were performed without primary antibodies and with matched species serum using similar immunoglobulin concentrations. For diaminobenzidine (DAB) staining of α-actinin-4 in mouse tissue, endogenous peroxidase activity was blocked with methanol supplemented with 0.3% peroxide after deparaffinization and rehydration. Heat-induced epitope antigen retrieval was performed in citrate (pH 6.0) and the same secondary antibodies were used as described above. Peroxidase activity was developed using a DAB+chromogen system (Dako). For quantification, digital images of the specimens were obtained using a Leica DFC500 digital camera mounted on a Leica DM5000B microscope. Image analysis was performed using Image-Pro Premier 9.0 (MediaCybernetics). Mean intensity of VectorRed (α-actinin-4) positivity in the VectorBlue (PECAM-1) positive areas was measured as optical density (OD). OD values of plaque and non-plaque regions of the same vessel (mouse tissue) or the same donor (human tissue) were compared.

Ex vivo confocal staining

Isolated arteries (aorta) and veins (left superior vena cava) were washed twice with PBS containing 1 mM $CaCl_2$ and 0.5 mM $MgCl_2$. Upon opening, vessels were fixed with 4% paraformaldehyde for 20 min at room temperature and stored in PBS containing 1 mM $CaCl_2$ and 0.5 mM $MgCl_2$ at 4℃. Blood vessels were permeabilized with 0.5% Triton X-100 and 5% glycerol for 10 min at room temperature, blocked with 2% BSA in PBS for 30 min at room temperature and washed with PBS containing 1 mM $CaCl_2$ and 0.5 mM $MgCl_2$ and incubated with primary [α-actinin-4, Alexa-488-labelled PECAM-1 (FAB3628G)] and secondary antibodies in 0.5% BSA and PBS each for 1 h at room temperature. After each step, the vessels were washed three times with PBS containing 1 mM $CaCl_2$ and 0.5 mM $MgCl_2$. The mounting was performed with Mowiol overnight at room temperature. Images were recorded with the Zeiss confocal microscope (63×/NA 1.4 oil objective).

Structural homology modelling

The structure homology model of the intracellular domain of human ICAM-1 (residues 503–532) was generated using the Phyre protein structure prediction server (Kelley and Sternberg, 2009). Top-scoring events were the structures of the intracellular domain of ICAM-2 (from the complex ICAM-2 with Radixin-FERM; PDB-ID, 1J19), the protein phosphatase subunit α4 (PDB-ID, 3QC1) and the PHAT domain (PDB-ID, 1OXJ). The figure was prepared with PyMOL (Molecular Graphics System, Schroedinger, LLC).

Statistical analysis

Mean±s.e.m. of the indicated number of independent experiments (n) were calculated. P-values were determined using an unpaired Student's t-test (Prism5). Statistical significance for the immunohistochemical stainings was determined by a paired Wilcoxon test and for the AFM data by a Mann–Whitney test. $P<0.05$ was considered as statistically significant.

Acknowledgements

We thank René van Lier (Sanquin Research, University of Amsterdam, The Netherlands) and Arnoud Sonnenberg (Netherlands Cancer Institute) for critical reading of the manuscript and Gijs van Schijndel (Sanquin Research, Amsterdam, The Netherlands) for technical assistance in the ELISA studies. We also thank Esther Lutgens, Arnoud Sonnenberg, Francisco Sanchez-Madrid, Alain Duperray and Ed Schuuring for providing materials.

Competing interests

The authors declare no competing interests.

Author contributions

A.S. designed and carried out most of the experiments; J.D.v.B. and P.L.H. conceived the study; J.t.R., K.R., M.H., E.C.A., E.P.J.M. and J.D.v.B. performed some experiments; A.S., J.t.R., K.R. and J.D.v.B analyzed data. C.J.d.V., M.J.D. and C.G.F. provided materials, expertise and access to equipment. A.S. and P.L.H. wrote the paper.

Funding

This work was supported by the Landsteiner Foundation for Blood Transfusion Research [grant number 903 to A.S. and M.H.]; the Dutch Heart Foundation [Dekker grant number 2005T039 to J.D.v.B]; and by a NWO Medium Sized Investment [NWO-ZonMW grant number 91110007 to J.t.R. and C.G.F.]. J.t.R. was also supported by a NWO-Veni grant [grant number 680-47-421] and C.G.F. was awarded with a NWO-Spinoza price and an ERC Advanced grant [PATHFINDER grant number 269019]. This work was also supported by the BioMedical Materials Institute [NEXTREAM research grant number P1.02 to C.J.d.V.], co-funded by the Dutch Ministry of Economic Affairs and the financial contribution of the Dutch Heart Foundation is gratefully acknowledged.

Supplementary material

Supplementary material available online at
http://jcs.biologists.org/lookup/suppl/doi:10.1242/jcs.154708/-/DC1

References

Barreiro, O., Yanez-Mo, M., Serrador, J. M., Montoya, M. C., Vicente-Manzanares, M., Tejedor, R., Furthmayr, H. and Sanchez-Madrid, F. (2002). Dynamic interaction of VCAM-1 and ICAM-1 with moesin and ezrin in a novel endothelial docking structure for adherent leukocytes. *J. Cell Biol.* **157**, 1233-1245.

Birukova, A. A., Arce, F. T., Moldobaeva, N., Dudek, S. M., Garcia, J. G., Lal, R. and Birukov, K. G. (2009). Endothelial permeability is controlled by spatially defined cytoskeletal mechanics: atomic force microscopy force mapping of pulmonary endothelial monolayer. *Nanomedicine* **5**, 30-41.

Bishop, A. L. and Hall, A. (2000). Rho GTPases and their effector proteins. *Biochem. J.* **348**, 241-255.

Carman, C. V., Sage, P. T., Sciuto, T. E., de la Fuente, M. A., Geha, R. S., Ochs, H. D., Dvorak, H. F., Dvorak, A. M. and Springer, T. A. (2007). Transcellular diapedesis is initiated by invasive podosomes. *Immunity* **26**, 784-797.

Carpén, O., Pallai, P., Staunton, D. E. and Springer, T. A. (1992). Association of intercellular adhesion molecule-1 (ICAM-1) with actin-containing cytoskeleton and alpha-actinin. *J. Cell Biol.* **118**, 1223-1234.

Celli, L., Ryckewaert, J. J., Delachanal, E. and Duperray, A. (2006). Evidence of a functional role for interaction between ICAM-1 and nonmuscle alpha-actinins in leukocyte diapedesis. *J. Immunol.* **177**, 4113-4121.

Courson, D. S. and Rock, R. S. (2010). Actin cross-link assembly and disassembly mechanics for alpha-Actinin and fascin. *J. Biol. Chem.* **285**, 26350-26357.

Craig, D. H., Haimovich, B. and Basson, M. D. (2007). Alpha-actinin-1 phosphorylation modulates pressure-induced colon cancer cell adhesion through regulation of focal adhesion kinase-Src interaction. *Am. J. Physiol.* **293**, C1862-C1874.

de Boer, O. J., van der Meer, J. J., Teeling, P., van der Loos, C. M., Idu, M. M., van Maldegem, F., Aten, J. and van der Wal, A. C. (2010). Differential expression of interleukin-17 family cytokines in intact and complicated human atherosclerotic plaques. *J. Pathol.* **220**, 499-508.

Ehrlicher, A. J., Nakamura, F., Hartwig, J. H., Weitz, D. A. and Stossel, T. P. (2011). Mechanical strain in actin networks regulates FilGAP and integrin binding to filamin A. *Nature* **478**, 260-263.

Etienne, S., Adamson, P., Greenwood, J., Strosberg, A. D., Cazaubon, S. and Couraud, P. O. (1998). ICAM-1 signaling pathways associated with Rho activation in microvascular brain endothelial cells. *J. Immunol.* **161**, 5755-5761.

Golji, J., Collins, R. and Mofrad, M. R. (2009). Molecular mechanics of the alpha-actinin rod domain: bending, torsional, and extensional behavior. *PLOS Comput. Biol.* **5**, e1000389.

Huynh, J., Nishimura, N., Rana, K., Peloquin, J. M., Califano, J. P., Montague, C. R., King, M. R., Schaffer, C. B. and Reinhart-King, C. A. (2011). Age-related intimal stiffening enhances endothelial permeability and leukocyte transmigration. *Sci. Transl. Med.* **3**, 112ra122.

Kanters, E., van Rijssel, J., Hensbergen, P. J., Hondius, D., Mul, F. P., Deelder, A. M., Sonnenberg, A., van Buul, J. D. and Hordijk, P. L. (2008). Filamin B mediates ICAM-1-driven leukocyte transendothelial migration. *J. Biol. Chem.* **283**, 31830-31839.

Kelley, L. A. and Sternberg, M. J. (2009). Protein structure prediction on the Web: a case study using the Phyre server. *Nat. Protoc.* **4**, 363-371.

Kirkbride, K. C., Sung, B. H., Sinha, S. and Weaver, A. M. (2011). Cortactin: a multifunctional regulator of cellular invasiveness. *Cell Adh. Migr.* **5**, 187-198.

Krause, M., te Riet, J. and Wolf, K. (2013). Probing the compressibility of tumor cell nuclei by combined atomic force-confocal microscopy. *Phys. Biol.* **10**, 065002.

Lessey-Morillon, E. C., Osborne, L. D., Monaghan-Benson, E., Guilluy, C., O'Brien, E. T., Superfine, R. and Burridge, K. (2014). The RhoA guanine nucleotide exchange factor, LARG, mediates ICAM-1-dependent mechanotransduction in endothelial cells to stimulate transendothelial migration. *J. Immunol.* **192**, 3390-3398.

Lin, D. C., Dimitriadis, E. K. and Horkay, F. (2007). Robust strategies for automated AFM force curve analysis – I. Non-adhesive indentation of soft, inhomogeneous materials. *J. Biomech. Eng.* **129**, 430-440.

Lyck, R., Reiss, Y., Gerwin, N., Greenwood, J., Adamson, P. and Engelhardt, B. (2003). T-cell interaction with ICAM-1/ICAM-2 double-deficient brain endothelium in vitro: the cytoplasmic tail of endothelial ICAM-1 is necessary for transendothelial migration of T cells. *Blood* **102**, 3675-3683.

Nourshargh, S., Hordijk, P. L. and Sixt, M. (2010). Breaching multiple barriers: leukocyte motility through venular walls and the interstitium. *Nat. Rev. Mol. Cell Biol.* **11**, 366-378.

Oakes, P. W., Patel, D. C., Morin, N. A., Zitterbart, D. P., Fabry, B., Reichner, J. S. and Tang, J. X. (2009). Neutrophil morphology and migration are affected by substrate elasticity. *Blood* **114**, 1387-1395.

Oh, H. M., Lee, S., Na, B. R., Wee, H., Kim, S. H., Choi, S. C., Lee, K. M. and Jun, C. D. (2007). RKIKK motif in the intracellular domain is critical for spatial and dynamic organization of ICAM-1: functional implication for the leukocyte adhesion and transmigration. *Mol. Biol. Cell* **18**, 2322-2335.

Phillipson, M., Heit, B., Colarusso, P., Liu, L., Ballantyne, C. M. and Kubes, P. (2006). Intraluminal crawling of neutrophils to emigration sites: a molecularly distinct process from adhesion in the recruitment cascade. *J. Exp. Med.* **203**, 2569-2575.

Raab, M., Swift, J., Dingal, P. C., Shah, P., Shin, J. W. and Discher, D. E. (2012). Crawling from soft to stiff matrix polarizes the cytoskeleton and phosphoregulates myosin-II heavy chain. *J. Cell Biol.* **199**, 669-683.

Riedl, J., Crevenna, A. H., Kessenbrock, K., Yu, J. H., Neukirchen, D., Bista, M., Bradke, F., Jenne, D., Holak, T. A., Werb, Z. et al. (2008). Lifeact: a versatile marker to visualize F-actin. *Nat. Methods* **5**, 605-607.

Roca-Cusachs, P., del Rio, A., Puklin-Faucher, E., Gauthier, N. C., Biais, N. and Sheetz, M. P. (2013). Integrin-dependent force transmission to the extracellular matrix by α-actinin triggers adhesion maturation. *Proc. Natl. Acad. Sci. USA* **110**, E1361-E1370.

Sato, M., Nagayama, K., Kataoka, N., Sasaki, M. and Hane, K. (2000). Local mechanical properties measured by atomic force microscopy for cultured bovine endothelial cells exposed to shear stress. *J. Biomech.* **33**, 127-135.

Schenkel, A. R., Mamdouh, Z. and Muller, W. A. (2004). Locomotion of monocytes on endothelium is a critical step during extravasation. *Nat. Immunol.* **5**, 393-400.

Schnoor, M., Lai, F. P., Zarbock, A., Kläver, R., Polaschegg, C., Schulte, D., Weich, H. A., Oelkers, J. M., Rottner, K. and Vestweber, D. (2011). Cortactin deficiency is associated with reduced neutrophil recruitment but increased vascular permeability in vivo. *J. Exp. Med.* **208**, 1721-1735.

Shulman, Z., Shinder, V., Klein, E., Grabovsky, V., Yeger, O., Geron, E., Montresor, A., Bolomini-Vittori, M., Feigelson, S. W., Kirchhausen, T. et al. (2009). Lymphocyte crawling and transendothelial migration require chemokine triggering of high-affinity LFA-1 integrin. *Immunity* **30**, 384-396.

Shulman, Z., Cohen, S. J., Roediger, B., Kalchenko, V., Jain, R., Grabovsky, V., Klein, E., Shinder, V., Stoler-Barak, L., Feigelson, S. W. et al. (2012). Transendothelial migration of lymphocytes mediated by intraendothelial vesicle stores rather than by extracellular chemokine depots. *Nat. Immunol.* **13**, 67-76.

Sluimer, J. C., Kisters, N., Cleutjens, K. B., Volger, O. L., Horrevoets, A. J., van den Akker, L. H., Bijnens, A. P. and Daemen, M. J. (2007). Dead or alive: gene expression profiles of advanced atherosclerotic plaques from autopsy and surgery. *Physiol. Genomics* **30**, 335-341.

Stossel, T. P., Condeelis, J., Cooley, L., Hartwig, J. H., Noegel, A., Schleicher, M. and Shapiro, S. S. (2001). Filamins as integrators of cell mechanics and signalling. *Nat. Rev. Mol. Cell Biol.* **2**, 138-145.

Stroka, K. M. and Aranda-Espinoza, H. (2011). Endothelial cell substrate stiffness influences neutrophil transmigration via myosin light chain kinase-dependent cell contraction. *Blood* **118**, 1632-1640.

te Riet, J., Katan, A. J., Rankl, C., Stahl, S. W., van Buul, A. M., Phang, I. Y., Gomez-Casado, A., Schön, P., Gerritsen, J. W., Cambi, A. et al. (2011). Interlaboratory round robin on cantilever calibration for AFM force spectroscopy. *Ultramicroscopy* **111**, 1659-1669.

Tracqui, P., Broisat, A., Toczek, J., Mesnier, N., Ohayon, J. and Riou, L. (2011). Mapping elasticity moduli of atherosclerotic plaque in situ via atomic force microscopy. *J. Struct. Biol.* **174**, 115-123.

van Buul, J. D., Allingham, M. J., Samson, T., Meller, J., Boulter, E., García-Mata, R. and Burridge, K. (2007a). RhoG regulates endothelial apical cup assembly downstream from ICAM1 engagement and is involved in leukocyte trans-endothelial migration. *J. Cell Biol.* **178**, 1279-1293.

van Buul, J. D., Kanters, E. and Hordijk, P. L. (2007b). Endothelial signaling by Ig-like cell adhesion molecules. *Arterioscler. Thromb. Vasc. Biol.* **27**, 1870-1876.

van Buul, J. D., van Rijssel, J., van Alphen, F. P., Hoogenboezem, M., Tol, S., Hoeben, K. A., van Marle, J., Mul, E. P. and Hordijk, P. L. (2010a). Inside-out regulation of ICAM-1 dynamics in TNF-alpha-activated endothelium. *PLoS ONE* **5**, e11336.

van Buul, J. D., van Rijssel, J., van Alphen, F. P., van Stalborch, A. M., Mul, E. P. and Hordijk, P. L. (2010b). ICAM-1 clustering on endothelial cells recruits VCAM-1. *J. Biomed. Biotechnol.* **2010**, 120328.

van Rijssel, J., Kroon, J., Hoogenboezem, M., van Alphen, F. P., de Jong, R. J., Kostadinova, E., Geerts, D., Hordijk, P. L. and van Buul, J. D. (2012). The Rho-guanine nucleotide exchange factor Trio controls leukocyte transendothelial migration by promoting docking structure formation. *Mol. Biol. Cell* **23**, 2831-2844.

Wójciak-Stothard, B., Williams, L. and Ridley, A. J. (1999). Monocyte adhesion and spreading on human endothelial cells is dependent on Rho-regulated receptor clustering. *J. Cell Biol.* **145**, 1293-1307.

Wozniak, M. A., Desai, R., Solski, P. A., Der, C. J. and Keely, P. J. (2003). ROCK-generated contractility regulates breast epithelial cell differentiation in response to the physical properties of a three-dimensional collagen matrix. *J. Cell Biol.* **163**, 583-595.

Yang, L., Kowalski, J. R., Yacono, P., Bajmoczi, M., Shaw, S. K., Froio, R. M., Golan, D. E., Thomas, S. M. and Luscinskas, F. W. (2006). Endothelial cell cortactin coordinates intercellular adhesion molecule-1 clustering and actin cytoskeleton remodeling during polymorphonuclear leukocyte adhesion and transmigration. *J. Immunol.* **177**, 6440-6449.